INSTITUT DE FRANCE
Académie des sciences

Comptes Rendus
Mécanique

Marwa Youssef and Anouar Nasr

Comparative study of fatigue assessment of defective material based on affected depth

Volume 350 (2022), p. 547-563

Published online: 1 December 2022

https://doi.org/10.5802/crmeca.141

Les Comptes Rendus. Mécanique *sont membres du Centre Mersenne pour l'édition scientifique ouverte*
www.centre-mersenne.org
e-ISSN : 1873-7234

Comptes Rendus
Mécanique
2022, Vol. 350, p. 547-563
https://doi.org/10.5802/crmeca.141

Historical article / *Article historique*

Comparative study of fatigue assessment of defective material based on affected depth

Marwa Youssef *, [a] **and Anouar Nasr** [a, b]

[a] LGM, ENIM, Université de Monastir, Avenue Ibn Eljazzar, Monastir 5019, Tunisia

[b] IPEIM, Université de Monastir, Avenue Ibn Eljazzar, Monastir 5019, Tunisia

E-mails: marwayousseff@gmail.com (M. Youssef), anouar.nasr@hotmail.fr (A. Nasr)

Abstract. In this work, we propose a comparative study of fatigue assessment of artificial surface defects based on affected depth (AD). The defect is assumed to be a void (semi-spherical, elliptical, or circumferential notches) on the surface of a material subjected to fatigue loading.

An elastic–plastic model of Chaboche is implanted in Abaqus to simulate the cyclic Finite Element (FE) calculations.

The AD model is exploited with Crossland, Dang Van, and Papadopoulos fatigue criteria to determine Kitagawa diagrams. The experimental data of the defective material C35 steel are used for model validation and comparison. The proposed comparative study of fatigue assessment provides interesting results.

Keywords. High-cycle fatigue, Affected depth, Fatigue criterion, Defect, Kitagawa diagram.

Manuscript received 19 April 2022, revised 4 July 2022 and 5 October 2022, accepted 18 October 2022.

1. Introduction

Various studies have aimed to provide different methods to predict the fatigue limit of notched material.

Benedetti *et al.* [1] used the Theory of Critical Distances (TCD) combined with the multiaxial fatigue criterion to predict the notch fatigue strength of ductile cast iron.

Different multiaxial criteria were adopted and combined with the TCD approach [2] to account for the notch sensitivity of the material. A comparative study showed that the Carpinteri criterion leads to a better fatigue prediction, considering different critical TCD lengths under Mode I and Mode III loads.

Endo and Yanase [3] suggested a method to assess the lower bound of the fatigue limit of ductile cast iron under combined loading. This approach evaluated the influence of microstructural inhomogeneities (graphite and small casting defects) and the multiaxial loading conditions on the fatigue strength.

Murakami [4] defined the defect size parameter, named $\sqrt{\text{area}}$, to interpret the influence of the geometry defect on the fatigue life of defective material. It is calculated by the root square

* Corresponding author.

of the projected area of the defect on the plane perpendicular to the direction of the maximal principal stress. He proposed an empirical approach based on fatigue experimental results and established a relationship between the High-Cycle Fatigue (HCF) limit, the parameter, and the material hardness. The application of Murakami's model was limited to uniaxial fatigue loading and it did not take into account other modes of loadings for different defect forms.

Subsequently, Endo *et al.* [5] suggested an extension of the approach put forward by Murakami for biaxial loads. A criterion was presented for the fatigue limit assessment of the defective material subjected to combined axial and torsional loadings. Based on experimental tests using specimens with hole defect (diameter was 100 or 500 μm), the criterion is validated and good results were obtained for different phases between axial and torsional loads.

Based on the method of Murakami, a new approach for predicting fatigue limit has been suggested by Borsato *et al.* [6] and has been applied on ductile cast iron with solidification notches, such as microshrinkage porosities or chunky and spiky graphite. Their proposed model explained the material properties, especially the yield strength and the ultimate strength, leading to a better prediction of the fatigue limit of ductile irons with different types of solidification defects.

Taylor *et al.* [7] developed the Critical Distance Method (CDM) to evaluate the fatigue limit for the cracked or notched material using the linear elastic fracture mechanics method. The authors proposed three methods to evaluate the fatigue limit of bodies containing a stress concentration: point method, line method, and area method. The point method consisted of comparing the maximal local stress at a single point to the smooth sample fatigue limit. However, the line method and the area method used a comparison between the average value of the maximal local stress along a line or over an area and the smooth sample fatigue limit. The CDM provides interesting results for the small notch.

After several fatigue tests on materials with defects, Nadot *et al.* [8] emphasized that the initiation of short cracks was at the tip of the defect and the propagation of cracks was perpendicular to the maximal principal stress direction. The Defect Stress Gradient (DSG) approach was suggested by Nadot to assess the fatigue life of defective C35 steel subjected to a multiaxial cyclic loading.

To describe the impact of a defect in the fatigue criterion, the authors introduced a stress gradient term. This technique then took into account the defect type, form, and size. The DSG method showed good results for defects from 100 μm to 1000 μm. However, this method was limited to full-size components using the Finite Element (FE) submodel.

Nasr *et al.* [9] used the hypothesis confirmed by Papadopoulos and Panoskaltsis [10] on the effect of the hydrostatic pressure gradient and the non-influence of the shear stress gradient. FE computations were utilized to evaluate this gradient over a distance equal to the size of the defect area at the tip of the defect. This method was applied only for spherical defects and it ignored elliptical defects.

Nasr *et al.* [11] put forward an approach that predicted the probabilistic HCF behavior of nodular cast iron. The criterion adopted was based on the gradient of the hydrostatic stress.

The assessment of the Crossland stress around the defect required numerical FE simulation for each size at different loading levels. To minimize the frequency of simulation by the FE, Nasr adopted the technique of response surfaces to affect the dispersion due to the defect size. After replacing FE calculations with the response surfaces method, the authors used the Monte Carlo algorithm to calculate reliability. The results obtained were in good agreement with the experimental results. This method was applied only for spherical defects and it ignores other forms of defects based on the Crossland criterion.

With the aim to investigate the influence of different geometries of the defect and stress gradient on fatigue strength, Morel *et al.* [12] proposed a comparison between defects.

A multiaxial criterion was used to predict the experimental results of the steel C35 subjected to tensile and torsion loads. The authors affirmed that the effect of stress gradient was more important than the effect of size and shape of the notch.

The main focus of our work is to propose a comparative study of fatigue assessment of defective material based on AD suggested by Nasr *et al.* [13]. The FE calculations are performed for C35 steel with spherical, elliptical, and circumferential defects for diverse sizes and different loadings which lead to determining the equivalent stress for three fatigue criteria near the defect.

The predictions are consistent with the experimental investigation. After that, a comparison is made between the AD models based on the three criteria.

2. Material

In this study, the experimental data of C35 steel are used to analyze the stress distribution close to the defect. A study carried out on the microstructure of this material by Billaudeau *et al.* [14] showed that this steel had two structural components: the perlite and the ferrite. The average grain size for each phase was 16 μm for the perlite and 22 μm for the ferrite (Figure 1).

The main mechanical properties and endurance limits of C35 steel are reported from the experimental research of Billaudeau *et al.* [16] (Table 1).

To investigate the impacts of the shape and size of the defect on the fatigue limit, artificial defects are inserted in the middle length of the fatigue specimens. The technique of electric

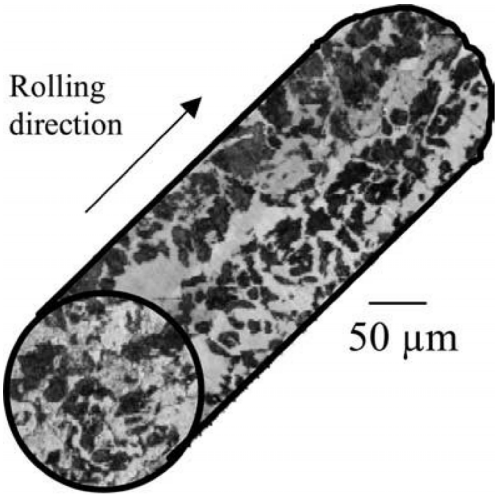

Figure 1. Representation of microstructure of steel C35 [15].

Table 1. Mechanical properties and endurance limits of C35 steel [16]

Young's modulus E (GPa)	212
Poisson's ratio ν	0.3
Monotonic yield strength $R_{p0.2}$ (MPa)	353
Cyclic yield strength $R_{p0.02\text{cy}}$ (MPa)	278
Tensile strength R_m (MPa)	582
Tension defect-free fatigue limit ($R=-1$) σ_{D-1} (MPa)	236 ± 12
Torsion defect-free fatigue limit ($R=-1$) τ_{D-1} (MPa)	169 ± 9

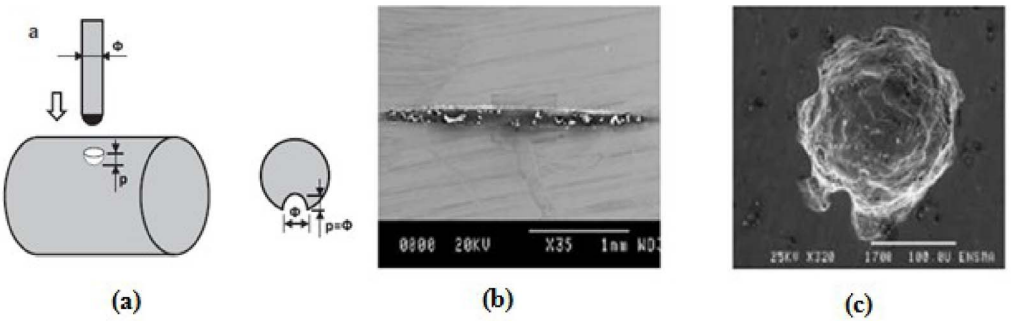

Figure 2. Scanning electron microscope image of defects introduced by spark-machining: (a) shape of electrode for the spherical defect; (b) elliptical defect; (c) spherical defect [14].

discharge machining [16] is applied to create artificial defects (Figure 2). This procedure permits reproducing defects and controlling shapes and sizes. The size varies in the (100 μm–1000 μm) range. To estimate the defect size, we refer to the Murakami parameter "$\sqrt{\text{area}}$" where the size is characterized by the root square of the "area" parameter ("area" of the projection of the defect projected onto the plane perpendicular to the direction of the maximal principal stress).

After introducing the defect, the C35 samples are tempered at 500° for one hour. This treatment relaxes residual stresses created during preparation.

3. HCF criteria

In this work, Crossland, Dang Van, and Papadopoulos HCF criteria are adopted with the AD concept to determine the fatigue strength of the defective material.

3.1. *Crossland criterion*

The Crossland criterion is used, and it is defined by the equivalent stress given by (1) [17]:

$$\sigma_{\text{eqCr}} = \sqrt{J_{2,a}} + \alpha_c P_{\max} \leq \beta_c \tag{1}$$

where $\sqrt{J_{2,a}}$ is the amplitude of the square root of the second invariant of the stress deviator obtained by a double maximization over the loading period (T):

$$\sqrt{J_{2,a}} = \frac{1}{2\sqrt{2}} \max_{t_i \epsilon T} \left\{ \max_{t_j \epsilon T} \sqrt{(\underline{\underline{S}}(t_i) - \underline{\underline{S}}(t_j)) : (\underline{\underline{S}}(t_i) - \underline{\underline{S}}(t_j))} \right\}. \tag{2}$$

In (2), $\underline{\underline{S}}(t_i)$ and $\underline{\underline{S}}(t_j)$ are the cyclic stress deviator tensors at two different instants t_i and t_j, and $P_{\max}$ is the maximal hydrostatic stress during a loading cycle calculated as follows (3):

$$P_{\max} = \tfrac{1}{3} \max_{t \epsilon T} \{\sigma_{11}(t) + \sigma_{22}(t) + \sigma_{33}(t)\}. \tag{3}$$

Material parameters α_c and β_c are identified from simple uniaxial tests (4) and (5): the fully reversed tension fatigue limit σ_{D-1} and the fully reversed torsion limit τ_{D-1}:

$$\alpha_c = 3\frac{\tau_{D-1}}{\sigma_{D-1}} - \sqrt{3} \tag{4}$$

$$\beta_c = \tau_{D-1}, \tag{5}$$

where σ_{D-1} denotes the fatigue limits of the defect-free material under fully reversed tension, and τ_{D-1} represents the fatigue limits of the defect-free material under fully reversed torsion.

3.2. *Dang Van criterion*

The Dang Van criterion is a stress-based multiaxial fatigue criterion. Dang Van proposed a combination of local shear $\tau(t)$ and hydrostatic stress $\sigma_H(t)$ [17].

Equation (6) is used to formulate the Dang Van criterion:

$$\sigma_{\text{eqDV}} = \max[\tau(t) + \alpha_{\text{DV}}\sigma_H(t)] \leq \beta_{\text{DV}}, \tag{6}$$

where α_{DV} and β_{DV} are material parameters defined using (7) and (8):

$$\alpha_{\text{DV}} = 3\left(\frac{\tau_{D-1}}{\sigma_{D-1}} - \frac{1}{2}\right) \tag{7}$$

$$\beta_{\text{DV}} = \tau_{D-1}, \tag{8}$$

where τ_{D-1} is the fatigue limit in fully reversed torsion and σ_{D-1} is the fatigue limit in fully reversed tension.

3.3. *Papadopoulos criterion*

Papadopoulos proposed a mesoscopic approach when the accumulated plastic strain under an external loading is evaluated at a scale on the order of a grain.

Papadopoulos suggested that the criterion would take the form of a linear combination of the maximal amplitude of the generalized shear stress T_a in the critical plane and the highest hydrostatic stress value σ_{hyd} in the mesoscopic scale [17].

Equation (9) presents the criterion.

$$\sigma_{\text{eqPap}} = \sqrt{\langle Ta^2 \rangle} + \alpha_{\text{Pap}}\sigma_{\text{hyd,max}} \leq \beta_{\text{Pap}}. \tag{9}$$

The constants β_{Pap} and α_{Pap} can be defined as (10) and (11):

$$\beta_{\text{Pap}} = \tau_{D-1} \tag{10}$$

$$\alpha_{\text{Pap}} = \frac{\frac{\sigma_{D-1} - \tau_{D-1}}{\sqrt{3}}}{\frac{\tau_{D-1}}{3}}. \tag{11}$$

4. FE simulation

The FE calculation carried out shows that the most stressed plane is the plane perpendicular to the direction of the maximal principal stress. In addition, previous studies [18] have claimed that the fatigue crack always initiates at the tip of the defect in the maximal shear plane. Therefore, consideration will be given to the variation in the fatigue equivalent stress near the defect. Defects are visualized on the sample surface subjected to torsion and tension loadings.

To simulate the stress distribution next to the defects, simplified models are proposed taking into account loading and geometric symmetries by using the commercial FE code ABAQUS [19].

Figure 3 illustrates the loads and boundary conditions of simplified parts under tension and torsion loadings.

Linear tetrahedral solid element C3D4 with four nodes is used for meshing a simplified part. Meshing is refined and optimized around the defects.

Figure 4 depicts the mesh employed during the use of a linear tetrahedral solid element with four-node C3D4.

An elastic–plastic model is adopted to simulate the cyclic FE calculations. The combined cyclic hardening behavior law is used to model the mechanical behavior of the material. It combines the isotropic and nonlinear kinematic hardening laws.

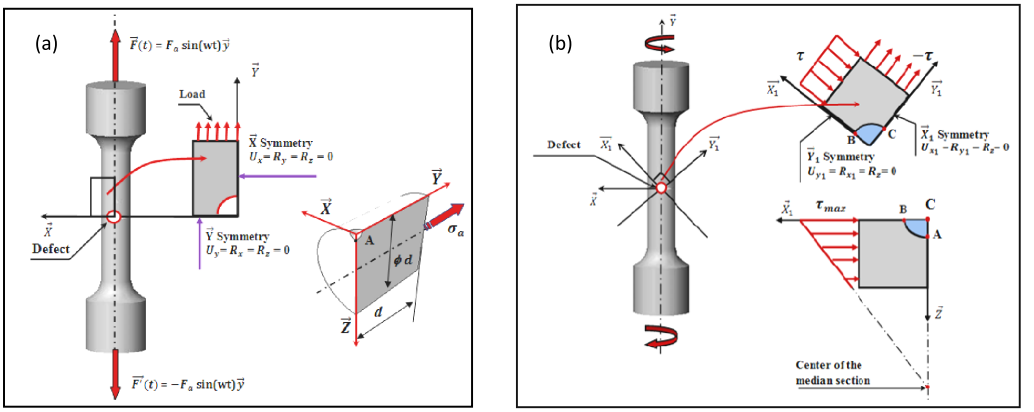

Figure 3. Completed and simplified model with load and boundary conditions: (a) tension loading; (b) torsion loading [13].

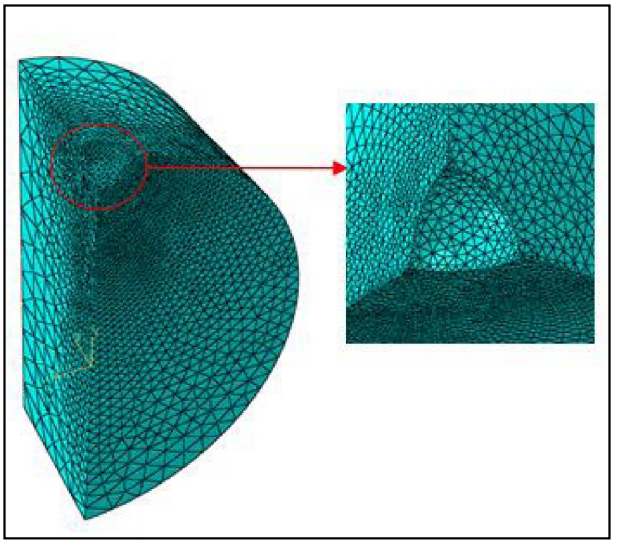

Figure 4. Refined mesh in front of a defect.

The cyclic behavior of C35 steel was studied by Gadouini *et al.* [20]. The tested specimens were subjected to imposed cyclic strain amplitudes.

The properties of the C35 steel for the EF calculation were extracted from the stress–deformation hysteresis curve, as illustrated in Figure 5.

5. Affected depth approach (background)

The AD approach was developed by Nasr *et al.* [13] for materials containing surface defects and subjected to periodic loadings. This approach calculated the fatigue limit of defective materials by using the HCF criteria. The authors proposed an AD a_w defined as the depth from the tip of the defect to the inside of the sample, where the Crossland criterion was violated. It was concluded that a_w was independent of the size of the defect. For each size of the defective material,

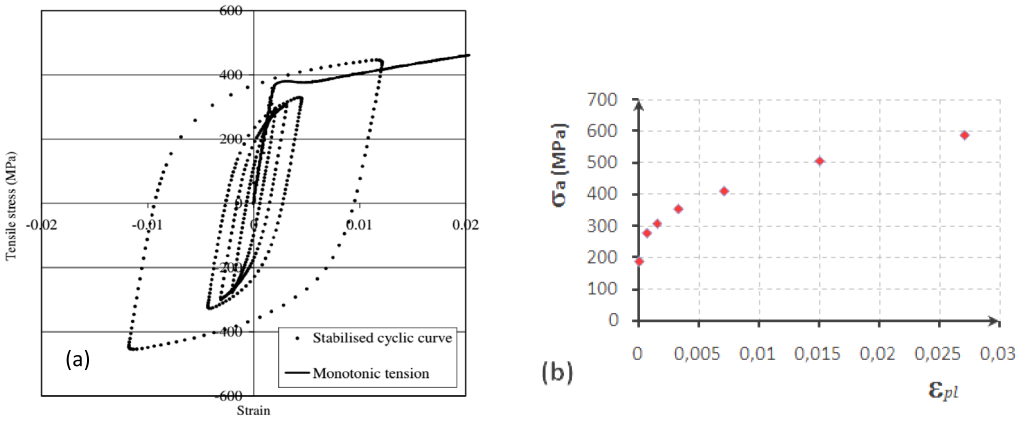

Figure 5. (a) Monotonic and cyclic tension curves, (b) plastic stress–strain cyclic stabilized curve (experimental result for the C35 material without defect) [20].

the fatigue limit could be evaluated by controlling the AD depending on the load amplitude, as given in the following model (12):

$$\sigma_{\text{eqCr}}(a_w) \leq \beta_c, \tag{12}$$

where $\beta_c = \tau_{D-1}$ is the fully reversed torsion fatigue limit of the defect-free material, and a_w is the parameter identified from one experimental fatigue limit of the defective material by numerical simulation.

Figure 6 shows the method proposed to evaluate the fatigue limit of material with defects under tensile or torsional loadings. First, we represent the simplified model. After determining the AD, the Crossland equivalent stress is calculated at a_w depth from the tip of the defect $\sigma_{\text{eqCr}}(a_w)$ and compared to β_c. If Crossland equivalent stress at the AD is greater than β_c ($\sigma_{\text{eqCr}}(a_w) > \beta_c$), the calculation will be repeated with an applied loading P less than that applied. If Crossland equivalent stress at the AD is less than β_c ($\sigma_{\text{eqCr}}(a_w) < \beta_c$), the calculation will be repeated with an applied loading P greater than that applied. The defective fatigue limit is obtained when the Crossland equivalent stress is equal to β_c.

6. Comparative study of criteria fatigue lifetimes based on affected depth

6.1. *Identification of affected depth for three criteria*

Based on the AD approach, we propose to determine the AD a_w of C35 for the three HCF criteria (Crossland, Dang Van, and Papadopoulos). This analysis allows us to estimate the AD as the depth from the tip of the defect into the interior of the specimen, which is subjected to its experimental defective fatigue limit where the fatigue equivalent stress is greater than $\beta_c = 169$ MPa.

Numerical simulation is applied to a sample with a spherical defect (size = $\sqrt{\text{area}} = 400$ μm), and it is subjected to its experimental defective fatigue limit equal to 150 MPa under the same tension loading at load ratio $R_\sigma = -1$. The acquired findings are illustrated in Figure 7.

Figure 7 depicts the equivalent stress distribution for three criteria for the same defect size subjected to the same tension loading near the fatigue limit for the same defect size. The equivalent stress exceeds the maximal value in front of the defect. It then focuses on decreasing the value until an asymptotically constant value is reached.

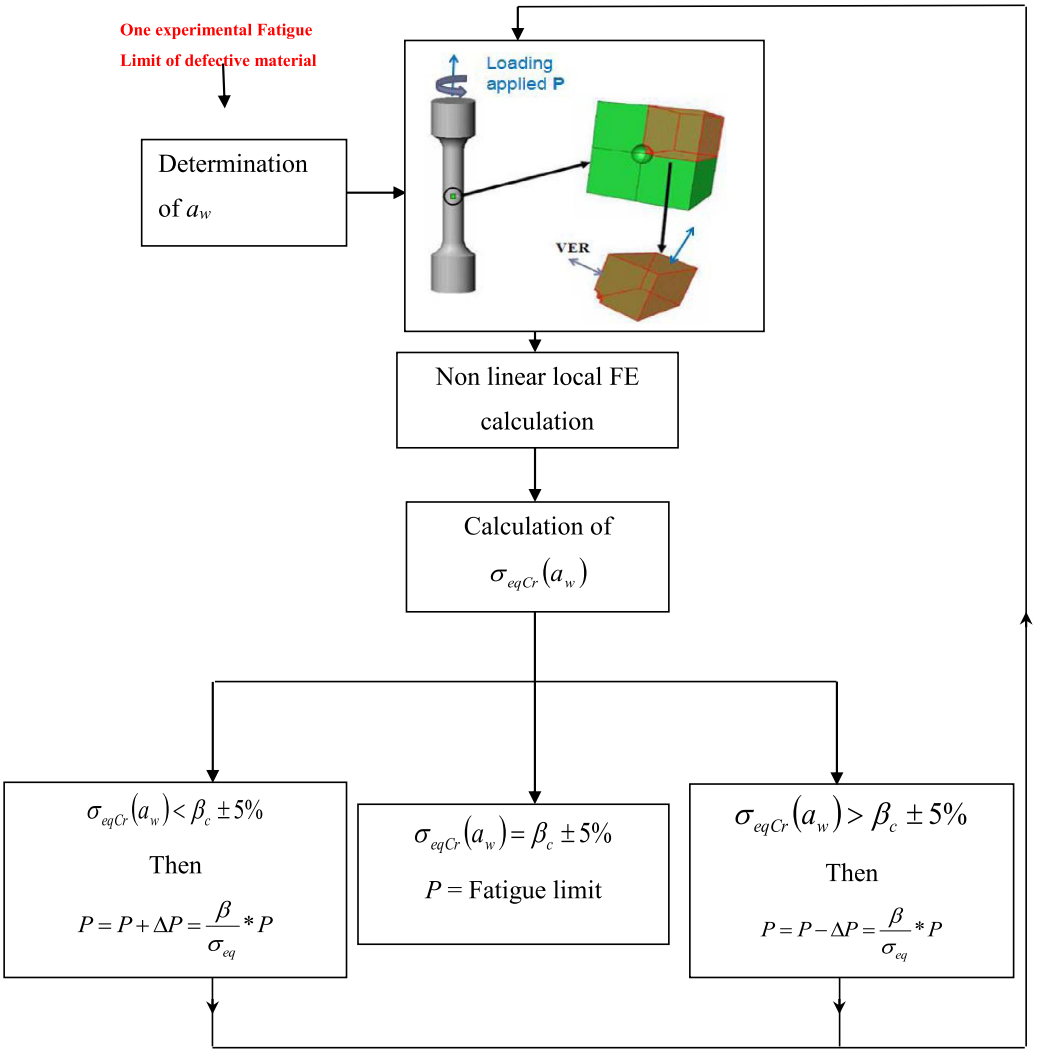

Figure 6. Iterative calculation to search for fatigue limit of a sample containing defect.

For the AD model based on Crossland criterion, the AD is about $a_{w\mathrm{Cr}}$ = 50 μm. The Dang Van equivalent stress reaches the value β_c at a depth equal to $a_{w\mathrm{DV}}$ = 40 μm. Hence, the AD corresponding to Papadopoulos criterion is equal to $a_{w\mathrm{Pap}}$ = 60 μm.

6.2. *Fatigue limit calculation based on three HCF criteria*

Kitagawa's diagram is simulated by the assessment of the fatigue limits for different defect sizes to validate the AD model. For the C35 material and the loading path, one experimental fatigue limit of the defective material is needed to identify the a_w parameter.

In previous investigations, Nasr *et al.* [13] showed that the AD parameter was independent of the defect shape. Therefore, for the elliptical void and the notched void, we keep the same a_w parameter corresponding to the spherical defect determined later.

Based on this finding, three HCF criteria are compared with the experimental tests employing three types of defects.

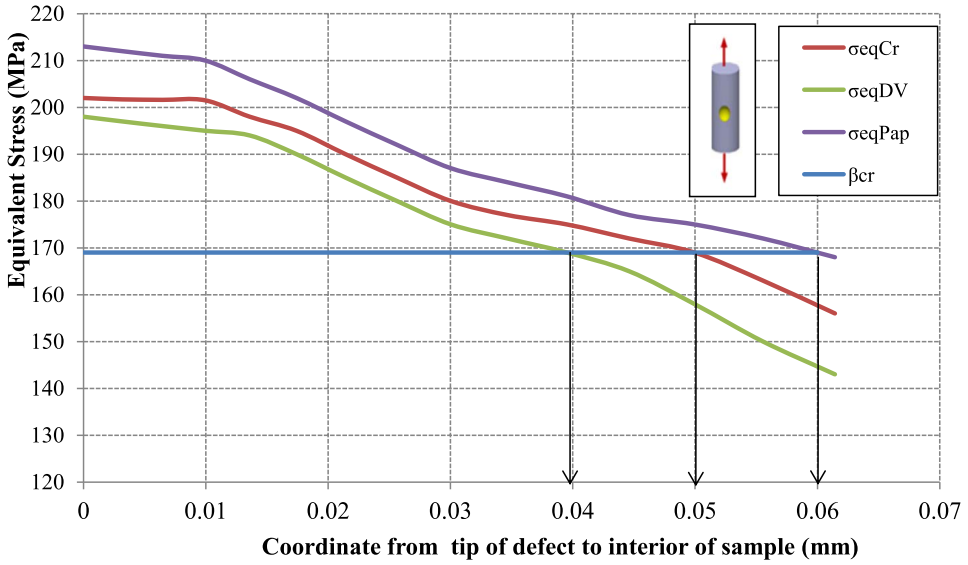

Figure 7. Equivalent stress distribution for three criteria under the same tension loading at load ratio $R_\sigma = -1$ ($\sigma_a = 150$ MPa and $\sqrt{\text{area}} = 400$ µm).

Table 2. Fatigue limits under torsion and tension loadings for different types of defects

Defect geometry	Loading	Defect size (µm)	Experimental fatigue limit (MPa)	Ref.
Spherical	Tension	170	195	[16]
		400	150	
		900	135	
	Torsion	170	160	
		400	145	
		900	125	
Elliptical transverse	Tension	170	200	
		400	155	
Elliptical longitudinal	Tension	40	236	
		170	225	
		370	220	
Circumferential	Tension	320	85	[12]
		730	90	
	Torsion	320	83	
		730	62	

Table 2 shows the results of fatigue tests of the C35 steel loaded in tension and torsion. The specimens are cycled on 10^7 cycles [16].

6.2.1. *Spherical defects*

To predict the fatigue life of spherically defective parts, two loading types are used. In this order, two Kitagawa diagrams are proposed for modeling the influence of spherical defects subjected to torsion and tension loadings.

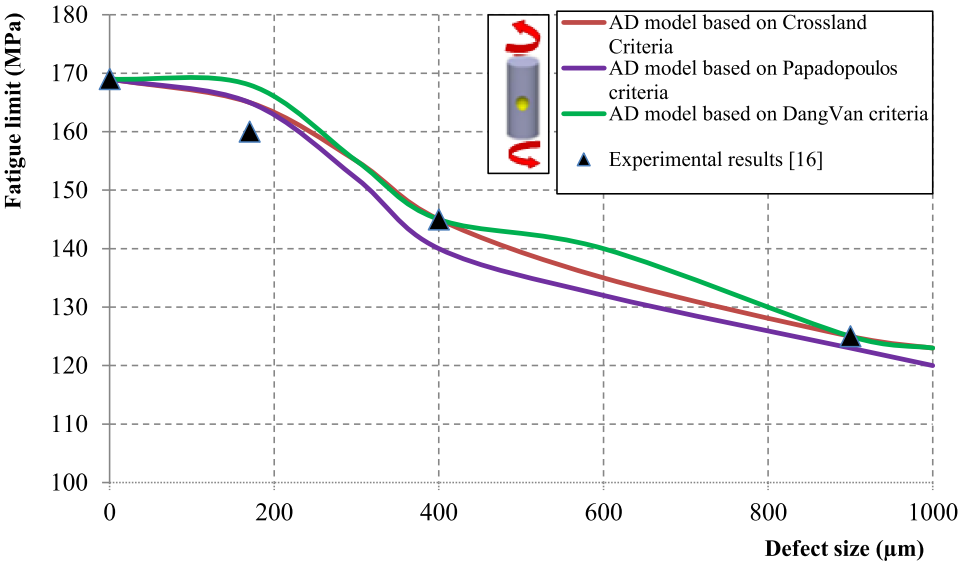

Figure 8. Kitagawa diagram using AD model for C35 steel subjected to fully reversed torsion at load ratio $R_\sigma = -1$, for spherical pore, for three HCF criteria compared with experimental results [16].

(a) *Fully reversed torsion loading* ($R_\sigma = -1$)

Figure 8 demonstrates the variation in the fatigue limit for C35 steel subjected to a fully reversed torsion stress for spherical defects using three HCF criteria as a function of the defect size.

(b) *Fully reversed tension loading* ($R_\sigma = -1$)

Figure 9 provides Kitagawa's diagram applied for defective C35 steel with a spherical pore to analyze the stress distribution under a tension loading at load ratio $R_\sigma = -1$ based on the three HCF criteria.

The results provided by Kitagawa's diagram (Figures 8 and 9) and applied for specimens containing spherical defects loaded in tension and torsion are as follows:

- The AD models based on the three HCF criteria lead to very encouraging results when compared to the experimental results [16].
- As the defect size increases, the fatigue limit decreases and tends towards an asymptotic value for both loading modes.
- The comparison of the three criteria with the experiments indicates that the AD model using the Crossland approach yields better correlation with the experimental results than that by Dang Van and Papadopoulos criteria for the spherical defect.

6.2.2. *Elliptical defects*

In order to validate the applicability of the suggested model in describing the effect of the shape of the defect, an AD model with an elliptical pore is adopted.

In this regard, two Kitagawa diagrams are utilized for modeling the influence of elliptical defects subjected to transversal and longitudinal dispersion tension loading.

(a) *Elliptical defect subjected to longitudinal dispersion tension loading*

Figure 10 presents Kitagawa's diagram carried out to estimate the fatigue limit around the elliptical defect subjected to tension loading with longitudinal dispersion.

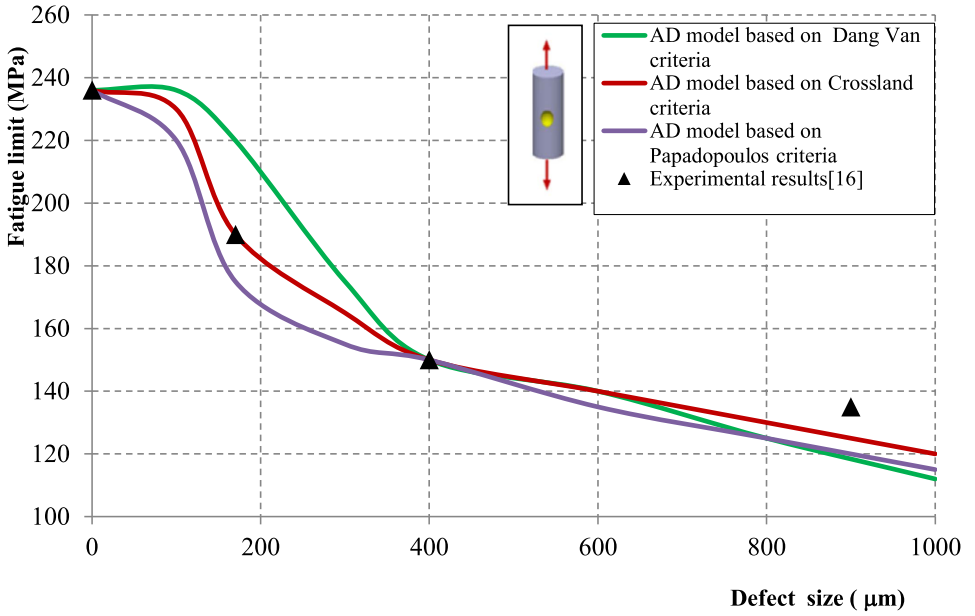

Figure 9. Kitagawa diagram using AD model for C35 steel subjected to fully reversed tension at load ratio $R_\sigma = -1$, spherical pore, for three HCF criteria compared with experimental results [16].

(b) *Elliptical defect subjected to tension loading with transverse dispersion*

Figure 11 compares the experimental results [16] and simulated Kitagawa–Takahashi's diagrams related to three HCF criteria for C35 steel with an elliptical transverse pore subjected to fully reversed tension.

The predictions observed in Figures 10 and 11 highlight the fact that:

- The proposed model provides good results for transverse elliptical defects and demonstrates that longitudinal defects do not affect the fatigue limit.
- The suggested model gives good results for transverse and longitudinal elliptical defects and proves that the AD model based on the Crossland criterion shows better correlations with experimental results.

6.2.3. *Circumferential notches*

Another shape of a defect is used to improve the proposed model. Figure 12 illustrates a simplified model using circumferential notches subjected to fully reversed tension and torsion.

(a) *Fully reversed torsion loading* ($R_\sigma = -1$)

The obtained results of the application of the AD model for the C35 steel containing circumferential notches subjected to torsion are illustrated in Figure 13.

(b) *Fully reversed tension loading* ($R_\sigma = -1$)

For defective C35 steel subjected to the tension load, predicted Kitagawa diagrams corresponding to circumferential notches are presented in Figure 14.

Figures 13 and 14 affirm that:

- For circumferential notches, the fatigue limits decline with the defect size and lead to an asymptotic value, similarly to tension and torsion loadings.

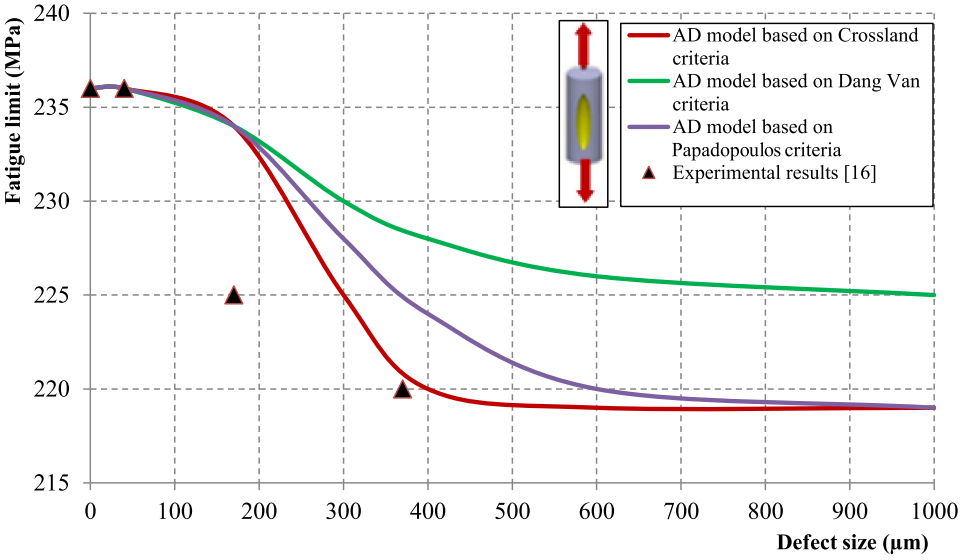

Figure 10. Kitagawa diagram using AD model for C35 steel subjected to fully reversed tension at load ratio $R_\sigma = -1$, for longitudinal elliptical pore, for three HCF criteria compared with experimental results [16].

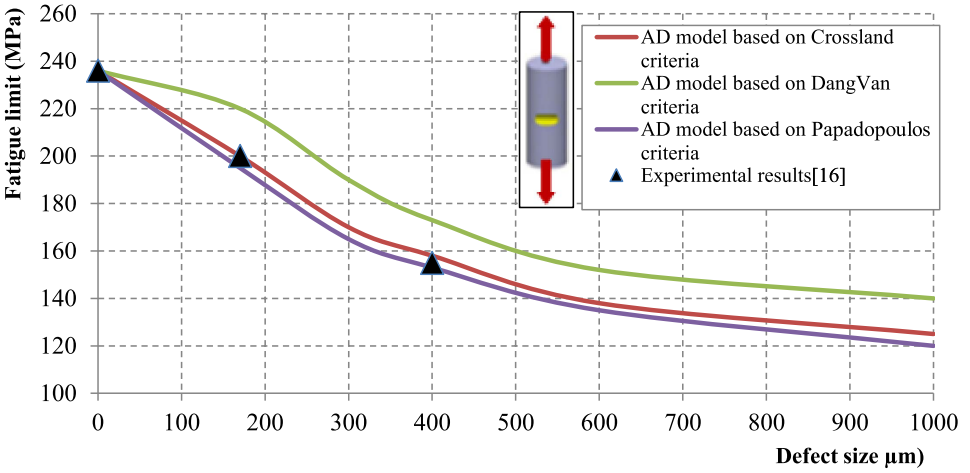

Figure 11. Kitagawa diagram using AD model for C35 steel subjected to fully reversed tension at load ratio $R_\sigma = -1$, for transverse elliptical pore, for three HCF criteria compared with experimental results [16].

- The comparison with the experimental results in [12] shows that the AD model can analyze the effect of the defect geometry on the fatigue strength.
- The comparison with the experimental results shows that the AD model based on Crossland applied to the C35 steel subjected to fully reversed tension with circumferential notches leads to better results.
- This comparative study of criteria fatigue lifetimes related to circumferential notches shows that the AD model based on Crossland leads to better results for both loading modes.

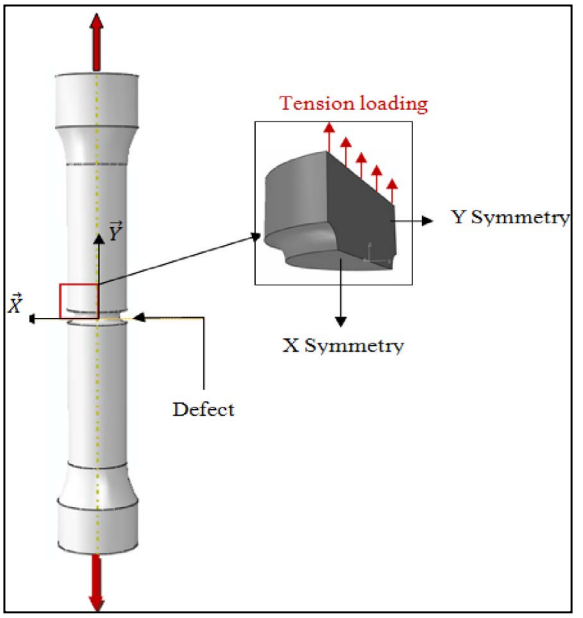

Figure 12. Simplified model with circumferential notches subjected to tension loading.

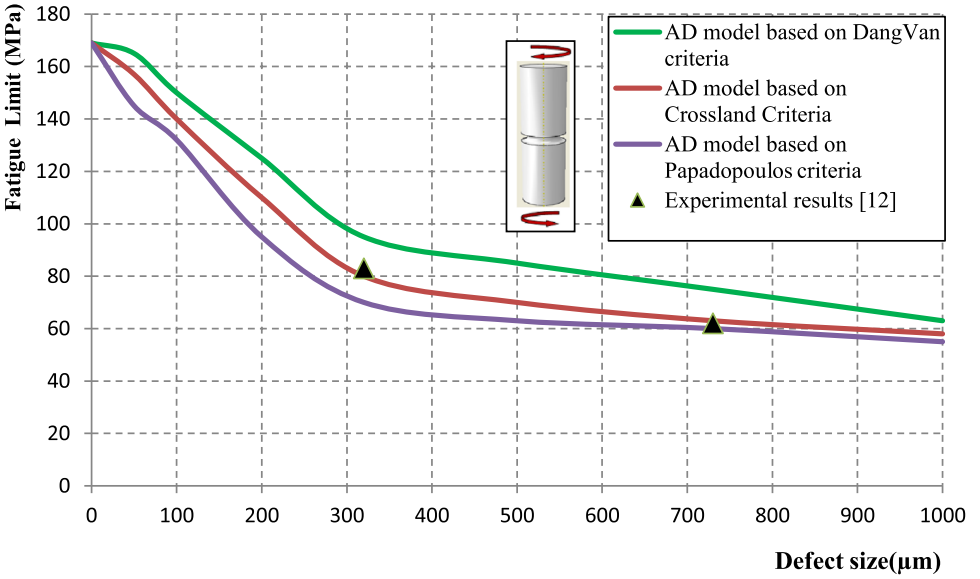

Figure 13. Kitagawa diagram using AD model for C35 steel subjected to fully reversed torsion at load ratio $R_\sigma = -1$, for circumferential notches, for three HCF criteria compared with experimental results [12].

7. Kitagawa diagram for spherical, elliptical, and circumferential notches

In order to study the influence of the morphology of the defect, three types of artificial defects are compared: spherical, elliptical, and circumferential.

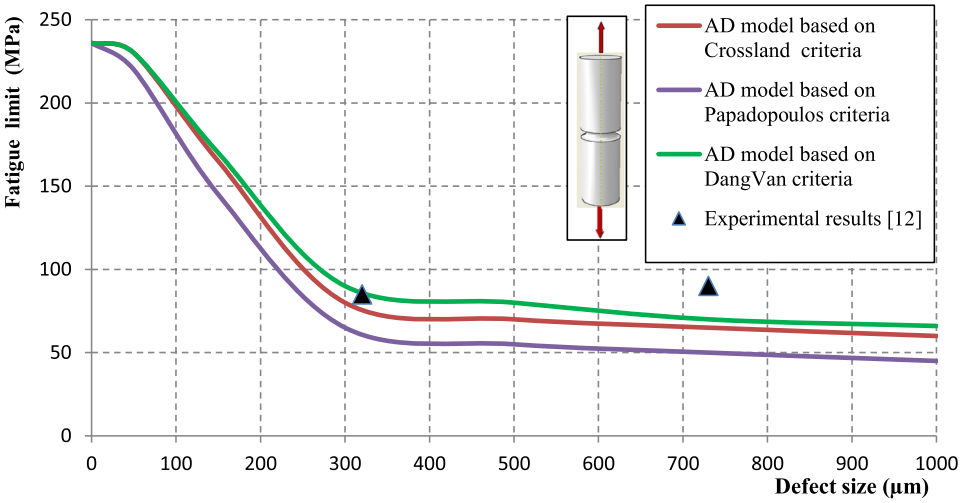

Figure 14. Kitagawa diagram using AD model for C35 steel subjected to fully reversed tension at load ratio $R_\sigma = -1$, for circumferential notches, for three HCF criteria compared with experimental results [12].

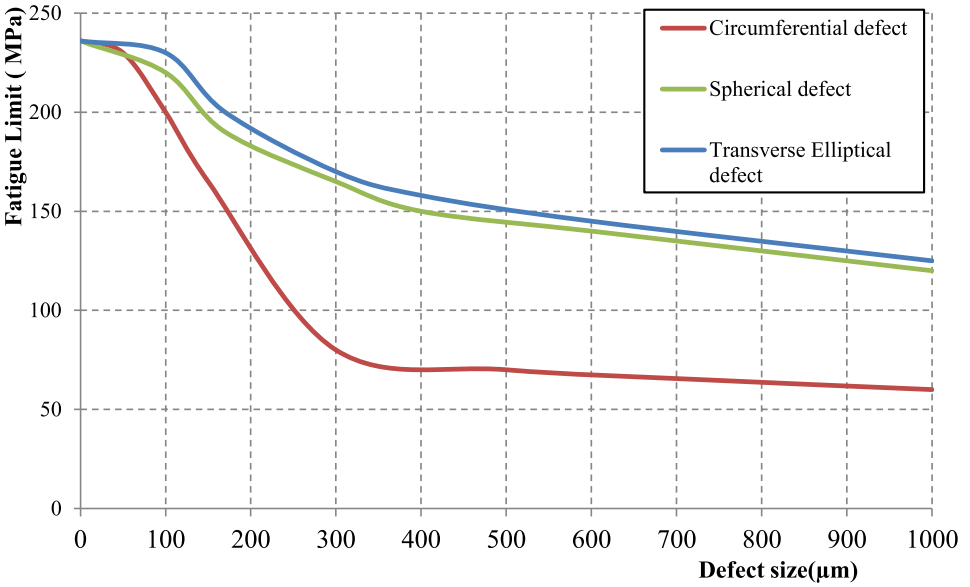

Figure 15. Kitagawa diagram using AD model based on Crossland criterion for C35 steel subjected to fully reversed tension at load ratio $R_\sigma = -1$.

Kitagawa–Takahashi diagrams are considered under tension loadings. The computed results are represented in Figure 15.

Figure 15 shows that for three defect types, Kitagawa–Takahashi diagrams present two different parts: (i) a first part for the small defects (size less than 400 µm) where the defect has a significant effect on the HCF limit and where it decreases as a function of the defect size, and (ii) a second part for the large defects (size goes from 400 µm to 1000 µm). For the second part, it is observed that by increasing the defect size, the HCF limit remains almost constant. This demonstrates that the defect size effect on the HCF limit decreases.

However, the Kitagawa diagrams prove that the transverse-elliptical and spherical fatigue limits are bigger than the circumferential limit. In addition, for the two defect types, transverse-elliptical and spherical, the stress distributions are very close, while for the circumferential defect they are lower.

It is noted that for a big circumferential notch, the defect-free fatigue limit is reduced by more than 75%, whereas it goes down by only 50% for the elliptical and spherical defects. It can be therefore concluded that the circumferential notch has an important effect and is much more significant on the C35 tension fatigue limits.

Consequently, and to better study the influence of the defect morphology, it appears necessary to estimate the stress concentration induced by different shapes of surface defects (circumferential notches, transverse elliptical pores, and spherical pores) on the fatigue strength.

Thus, numerical simulation is conducted to determine the elastic–plastic stress concentration factor Kt at a highly loaded point.

It is observed that Kt is equal to 2 all over the equator of the spherical pore on the plane perpendicular to the tension direction. For the transverse elliptical pore, Kt reaches the value 2.4 at the maximal loaded point (the tip of the defect). Finally, the stress concentration factor of the circumferential notches is the highest, where Kt is about 3.5 at the maximal loaded point.

To sum up, the fatigue limit is affected by the circumferential defect earlier than the elliptical and spherical pores. Hence, it is important to note that the AD approach properly explains the effect of the morphology of the defect.

8. Conclusion

In this study, the fatigue life assessment has been conducted based on the concept of the AD approach and has been applied to the defective C35 material under cyclic loading.

To illustrate the morphology influence of the defect, three types of defects (spherical, elliptical, and circumferential notches) have been considered.

Simplified FE models considering loading and geometry symmetries have been generated to find out the stress distribution near the defect subjected to torsion and tension loadings at a load ratio $R_\sigma = -1$.

The AD approach has been used to predict the Kitagawa–Takahashi diagrams for three void types using three multiaxial fatigue criteria Crossland, Dang Van, and Papadopoulos.

For each type and size of a defect, only one experimental fatigue limit for C35 steel has been needed to assess all fatigue limits under tension or torsion loadings at a load ratio $R_\sigma = -1$.

Then, the computed results have shown a good agreement with the experimental investigations and confirmed that the AD parameter can characterize the effect of defects on the fatigue behavior for diverse defect types.

In addition, this approach can be developed with different HCF criteria and can evaluate the fatigue resistance of defective materials.

The comparison of the three AD models based on three criteria with the experimental results has indicated that the predicted Crossland approach provides better correlations with the experimental results for a different defect type than that by Dang Van and Papadopoulos criteria.

Finally, to investigate the influence of the defect morphology, three types of artificial defects have been compared: spherical, elliptical, and circumferential. Moreover, the stress concentration induced by different shapes of surface defects has been evaluated.

The defect has been simply modeled by a surface void. It will be interesting to try to find other defect models to come closer to the natural defect morphology. It is very important to study the performance of the AD parameter against other types of materials with various structures and proprieties.

The results have been obtained for only three types of defects, so it will be significant to test the AD model for materials containing other types of defects such as the circumferential V-notch, the inclusion, and the drilled holes.

In this work, the defect has been just tested under pure tension and pure torsion with constant amplitude loadings. Some perspectives of this study are to validate the AD approach for defective materials subjected to complex multiaxial loadings such as combined tension and torsion loadings, as well as variable amplitude loading conditions.

Nomenclature

$\sqrt{\text{area}}$	Equivalent defect size of defect perpendicular to the direction of the maximum principal stress (μm)
HCF	High-Cycle Fatigue
a_w	Affected depth at fatigue limit (μm)
$a_{w\text{Cr}}$	Affected depth for Crossland criterion (μm)
$a_{w\text{DV}}$	Affected depth for Dang Van criterion (μm)
$a_{w\text{Pap}}$	Affected depth for Papadopoulos criterion (μm)
E	Young's modulus (GPa)
R_m	Ultimate tensile strength (MPa)
$R_{p0.2}$	0.2% monotonous yield stress (MPa)
$R_{p0.02\text{cy}}$	0.2% cyclic yield stress (MPa)
R_σ	Load ratio: $R_\sigma = \sigma_{\min}/\sigma_{\max}$
ν	Poisson's ratio
$J_{2,a}$	Amplitude over load cycle of the second invariant of deviatoric stress tensor (MPa^2)
$\underline{\underline{S}}(t_i)$ and $\underline{\underline{S}}(t_j)$	The periodic deviator stress tensor in two diverse instants (t_i and t_j)
$P_{\max}$	Is the maximal hydrostatic stress during a loading cycle (MPa)
σ_a	Amplitude of tension loading (MPa)
σ_{D-1}	Fatigue limit under fully reversed tension of defect-free material (MPa)
τ_a	Amplitude of torsion loading (MPa)
τ_{D-1}	Fatigue limit under fully reversed torsion of defect-free material (MPa)
α_c	Coefficient in Crossland criterion
β_c	Material parameter in Crossland criterion (MPa)
α_{DV}	Coefficient in Dang Van criterion
β_{DV}	Material parameter in Dang Van criterion (MPa)
$\tau(t)$	Local shear (MPa)
$\sigma_H(t)$	Hydrostatic stress (MPa)
α_{Pap}	Coefficient in Papadopoulos criterion
β_{Pap}	Material parameter in Papadopoulos criterion (MPa)
σ_{hyd}	Hydrostatic stress value (MPa)
T_a	The generalized shear stress (MPa)
σ_{eqCr}	Crossland equivalent stress (MPa)
σ_{eqDV}	Dang Van equivalent stress (MPa)
σ_{eqPap}	Papadopoulos equivalent stress (MPa)
Kt	Elastic–plastic stress concentration factor

Conflicts of interest

Authors have no conflict of interest to declare.

References

[1] M. Benedetti, C. Santus, S. Raghavendra, D. Lusuardi, F. Zanini, S. Carmignato, "Multiaxial plain and notch fatigue strength of thick-walled ductile cast iron EN-GJS-600-3: Combining multiaxial fatigue criteria, theory of critical distances, and defect sensitivity", *Int. J. Fatigue* **156** (2022), article no. 106703.

[2] D. Taylor, *The Theory of Critical Distances. A New Perspective in Fracture Mechanics*, 1st ed., Elsevier Science, Oxford, UK, 2007.

[3] M. Endo, K. Yanase, "Effects of small defects, matrix structures and loading conditions on the fatigue strength of ductile cast irons", *Theor. Appl. Fract. Mech.* **69** (2014), p. 34-43.

[4] Y. Murakami, *Metal Fatigue, Effects of small Defects and Nonmetallic Inclusion*, Elsevier Science Ltd, Oxford, UK, 2002.

[5] M. Endo, I. Ishimoto, "The fatigue strength of steels containing small holes under out of phase combined loading", *Int. J. Fatigue* **28** (2006), no. 5–6, p. 592-597.

[6] T. Borsato, P. Ferro, F. Berto, "Novel method for the fatigue strength assessment of heavy sections made by ductile cast iron in presence of solidification defects", *Fat. Fract. Eng. Mater. Struct.* **41** (2018), no. 8, p. 1746-1757.

[7] D. Taylor, L. Susmel, "Two methods for predicting the multiaxial fatigue limits of sharp notches", *Fat. Fract. Eng. Mater. Struct.* **26** (2003), p. 821-833.

[8] Y. Nadot, T. Billaudeau, "Multiaxial fatigue limit criterion for defective materials", *Eng. Fract. Mech.* **73** (2006), no. 1, p. 112-133.

[9] A. Nasr, "Fiabilité en fatigue polycyclique des matériaux a défaut sous chargement multiaxial", PhD Thesis, Ecole Polytechnique X, 2009.

[10] I. V. Papadopoulos, V. P. Panoskaltsis, "Invariant formulation of a gradient dependent multiaxial high cycle fatigue criterion", *Eng. Fract. Mech.* **55** (1996), no. 4, p. 513-528.

[11] A. Nasr, Ch. Bouraoui, R. Fathallah, Y. Nadot, "Probabilistic high cycle fatigue behavior of nodular cast iron containing casting defects", *Fat. Fract. Eng. Mater. Struct.* **32** (2009), p. 292-309.

[12] F. Morel, A. Morel, Y. Nadot, "Comparison between defects and micro-notches in multiaxial fatigue—The size effect and the gradient effect", *Int. J. Fatigue* **31** (2009), no. 2, p. 263-275.

[13] A. Nasr, W. Hassine, Ch. Bouraoui, "Fatigue limit assessment for defective materials based on affected depth", *Met. Res. Technol.* **114** (2017), article no. 505.

[14] T. Billaudeau, "Fatigue multiaxiale des matériaux à défauts: mécanismes et critère d'endurance", PhD Thesis, ENSMA, Poitiers, 2002.

[15] L. Flaceliere, "Contribution à la modélisation du dommage en fatigue multiaxiale d'un acier C36 : Confrontation a l'experience", PhD Thesis, ENSMA, Poitiers, 2004.

[16] T. Billaudeau, Y. Nadot, G. Bezine, "Multiaxial fatigue limit for defective materials: mechanisms and experiments", *Acta Mater.* **52** (2004), p. 3911-3920.

[17] M. Ciavarella, F. Monno, "A comparison of multiaxial fatigue criteria as applied to rolling contact fatigue", *Int. J. Fatigue* **43** (2010), p. 2139-2144.

[18] A. Nasr, Y. Nadot, Ch. Bouraoui, R. Fathallah, M. Jouiad, "Fatigue initiation in C35 steel: Influence of loading and defect", *Int. J. Fatigue* **32** (2010), p. 780-787.

[19] K. Hibbit, Sorenson, Inc., *Abaqus User's Manual Version 6.2*, HKS, Pawtucket, RI (USA), 2001.

[20] H. Gadouini, Y. Nadot, C. Rebours, "Influence of mean stress on the multiaxial fatigue behavior of defective materials", *Int. J. Fatigue* **30** (2008), no. 9, p. 1623-1633.